[SSC19-WKVIII-04]

Folded Lightweight Actuator Positioning System (FLAPS)

Paula do Vale Pereira, Katherine S. Chun, Mario M. Contreras, Charles Lindsay, Shreeyam Kacker, Raymond Huffman, Christian Haughwout, Kerri Cahoy
Massachusetts Institute of Technology, Department of Aeronautics and Astronautics, Space Telecommunications, Astronomy, and Radiation Laboratory
77 Massachusetts Avenue, 37-315, Cambridge, MA 02139; (617) 253-7805
paulavp@mit.edu

ABSTRACT

Precision actuation of mechanical structures on small spacecraft is challenging. Current solutions include single-use actuators, which rely on pyrotechnics and springs, and multiple-use actuators, which typically consume more size, weight, and power than available on CubeSats. The Folded Lightweight Actuated Positioning System (FLAPS) demonstrates the use of a simple rotary shape memory alloy (SMA) actuator in a bending architecture, along with a feedback control loop for repeatable and precise deployment. The FLAPS mechanism consists of a pair of SMA strips mounted to a hinge assembly, with one side attached to the CubeSat bus and the other to the deployable element. A custom actuator shape was manufactured using oven annealing. SMA actuation is achieved using joule heating. Feedback control is provided by a closed-loop PID control scheme, feedback sensor, and controller board. The FLAPS actuator is currently being developed for CubeSat solar panel positioning and drag control. Other potential FLAPS applications include aperture repositioning, deployable radiators, and steerable antennas. The FLAPS team will validate the actuator system in a microgravity environment on a parabolic flight in late 2019.

INTRODUCTION

Many challenges facing small satellites are due to limitations in size, weight, and power (SWaP). Deployable mechanisms can overcome some of the SWaP limitations by allowing larger structures to launch aboard smaller spacecrafts. However, deployables typically add complexity and cost, becoming a critical component of the mission architecture. This paper outlines the development of a compact SMA hinge that provides repeatable and precise actuation and can be used on small satellites such as CubeSats.

Motivation

The goal of this work is to develop a compact, precise, and efficient multiple-use actuator. There are two types of actuators: single-use and multiple-use. Single-use actuators are historically reliable and compact, but limited to a single deployed position and do not support additional adjustments.[1] Pyrotechnic actuators involve a device held under tension and released when the mechanism is broken or activated by the pyrotechnic element.[2] Some other single-use actuator types include springs, tapes, or booms.[1]

Multiple-use actuators are usually dependent on complex active elements such as motors, or gearboxes. Multiple-use actuators tend to be heavy and complex, which poses a problem for resource constrained small satellites.[1]

SMAs provide a mechanically simple and lightweight alternative for deploying payloads on power and space-constrained platforms due to their shape memory attributes.[3,4] Nitinol in particular is 25 times more work dense than an electric motor and is able to lift more than 100 times its weight.[5] SMAs are a well-characterized popular option for single-use actuators on spacecraft. TiNi Aerospace developed the Frangibolt, which has a SMA cylinder that breaks a bolt mechanism and releases the deployable.[6] Guzik and Benafan designed a SMA retention and release mechanism for body-mounted solar arrays on CubeSats.[7] Sierra Nevada offers the K-truss boom, which uses an elastic deployable boom for a single deployment.[8] Repeatable actuators are typically implemented in axial compression with a SMA wire contracting in length, facilitating complex movements via power transmission elements.[9,10]

Controlling SMA mechanisms is an additional challenge due to the hysteresis and nonlinear nature of the material.[11] To the best of the authors' knowledge, SMAs actuated in a bending architecture have not been implemented with a controller until this work.[12] We address the technical gap in lightweight, precise, and repeatable SMA actuators in a bending architecture with feedback control.

Objective

We extend previous work on SMA actuators at MIT by Khatsenko's open-loop rotary SMA actuator, which aimed to repeatably actuate a solar panel by constraining two SMA strips trained in opposite directions.[13] The mechanism was made of rectangular SMA strips bolted to the CubeSat body and solar panel, demonstrating the ability of SMA plates or foils to actuate to large angles. The SMAs were actuated with Joule heating and achieved the desired 90° actuation in a laboratory environment.

The FLAPS hinge aims to implement a similar SMA strip design in a bending architecture with feedback control to provide reliable actuation to multiple angles. A supporting hinge is included to help isolate the movement of the SMA strips. Actuation of the hinge in microgravity will be tested on a parabolic flight in late 2019.

APPROACH

The FLAPS approach involves using SMA strips with a supporting hinge structure, a magnetic encoder to track the hinge angle, and a small interface board for the sensing and control circuitry.

Mechanical Design

The hinge design discussed in this work has two separate halves joined by a low-friction pin-bushing interface. The shape memory alloy actuators are placed on the neutral axis of the hinge mechanism in order to minimize the bending strain the actuators experience. Two actuators are placed in the hinge to allow repeatable movement in two directions: one strip actuates to deploy the mechanism, and the other strip brings it back to the stowed position. The two strips can also be used in opposition to achieve more precise position control. Fig. 1 schematically shows how the two strips actuate.

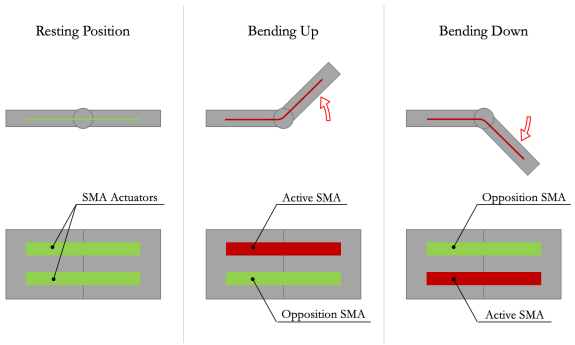

Figure 1: Schematics of the opposition hinging motion of the SMA actuators.

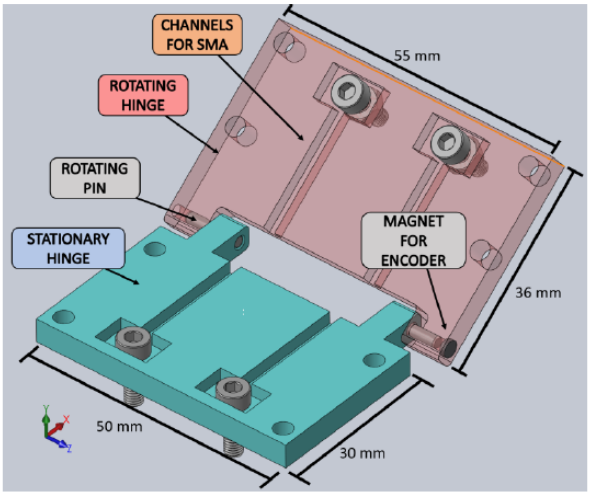

Figure 2: Original hinge design without buckling straps.

A magnetic encoder and its embedded magnet are used to read the hinge angular position.[14] For rapid prototyping purposes, the hinge is 3D-printed. We used a MarkForged printer and a nylon-carbon fiber composite material called Onyx due to its melting temperature above the 80°C SMA transition temperature.[15] Bolts attach the SMA actuators to the hinge and also attach the hinge to the CubeSat bus and the actuated surface. Fig. 2 shows the first iteration of the hinge design and indicates the positioning of the encoder and the SMA actuators.

To help prevent buckling, an extra element was added on the top of the strip, close to the bending axis, to maintain the strip as close as possible to the hinge. These are called "buckling straps", and they increase the actuation angle of the hinge by 80%. The mechanism setup with magnetic encoder, buckling straps, hinge, and SMA, is shown in Fig. 3.

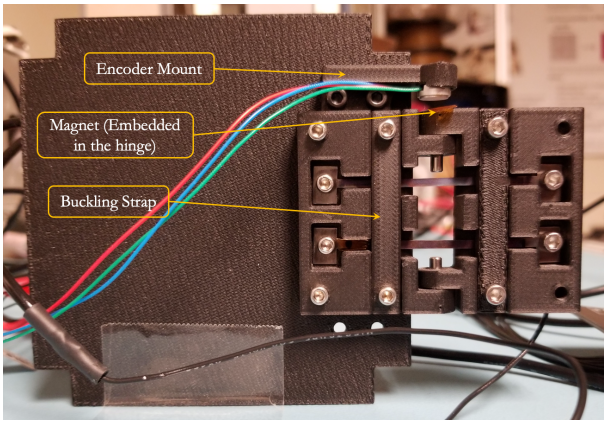

Figure 3: FLAPS hinge prototype.

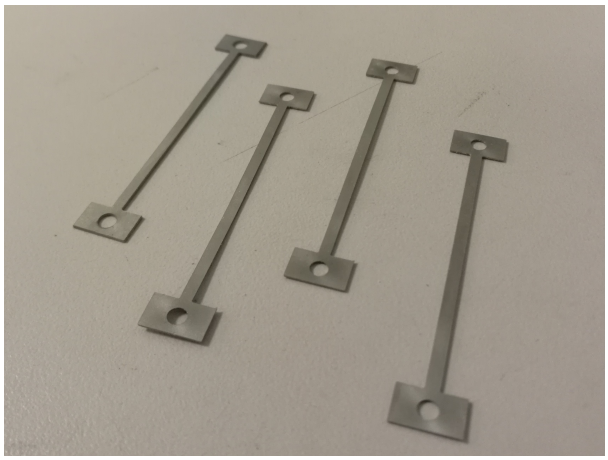

Figure 4: Nitinol SMA Strips with 62 mm length and 2 mm width.

The bending force of the SMA strip is derived from how much the material compresses or stretches as a function of its Young's Modulus, as can be seen in Eq. 1. The bending resistance of an SMA is derived from the beam deflection caused by a moment applied to the beam, as shown in Eq. 2. For this calculation, we assume that the SMA behaves as a weightless cantilever beam with the force being applied on the other end of the beam.[16] This means that the force applied by the actuated SMA is proportional to the thickness of the SMA (plus some extra influence due to the actuation angle, which is proportional to the thickness), whereas the resistance offered by the non-actuated SMA is proportional to the cube of the thickness:

$$F_{applied} = AE\frac{\Delta L}{L_0}\sin(\alpha), \tag{1}$$

$$F_{resistance} = \frac{Eb\delta}{4}\left(\frac{h}{L_0}\right)^3, \tag{2}$$

where A is the cross-sectional area of the actuator in m^2, E is the Young's Modulus of the SMA in Pa, L is the length of the actuator in m, α is the actuation angle in rad, b is the width of the cross-section of the actuator in m, and h is the height of the cross-section of the actuator in m. When the SMA strips are placed in opposition to each other in the hinge, the force exerted by one strip must overcome the resistance of the opposing strip. Thus, the appropriate cross-sectional geometry must be selected to maximize the actuation range of the entire hinge. The chosen geometry was a rectangular cross-section with a thickness that can be tuned for maximum actuation force without changing the geometry of the hinge. The rectangular cross-section also allows a better directionality of movement.

Shape Memory Alloy Manufacturing Process

Nitinol was selected as the SMA material based on its transition temperature range, commercial availability, and previous use in actuators for space applications.[2] Nitinol transition temperatures are well-defined and typically range from 0°C to 90°C. A transition temperature of 80°C was chosen to avoid the superelastic effects exhibited by Nitinol with a transition point near room temperature.[17] Higher transition temperatures also provide some built-in resistance to heat fluctuation onboard the spacecraft.

A rectangular "dog-bone" shape with holes at either end was water jetted out of a Nitinol plate, shown in Fig. 4. A flat plate was selected over the more common round wires since it provided a smaller area moment of inertia, making it easier for the opposing SMA to bend against it. It also made water jetting a mounting hole possible, providing a reliable mechanical and electrical connection. The additional width at either side of the strip improved the electrical contact with the screw that fastened the strip to the hinge. The narrower width in the middle section required less current to Joule heat the SMA strip to actuation.

After water jetting, the SMAs were annealed in an oven for 30 minutes at 500°C. The oven is located at the MIT Glass Lab and is typically used to anneal glassware after the blowing process. The oven is constantly maintained at 500°C. To train the SMAs,

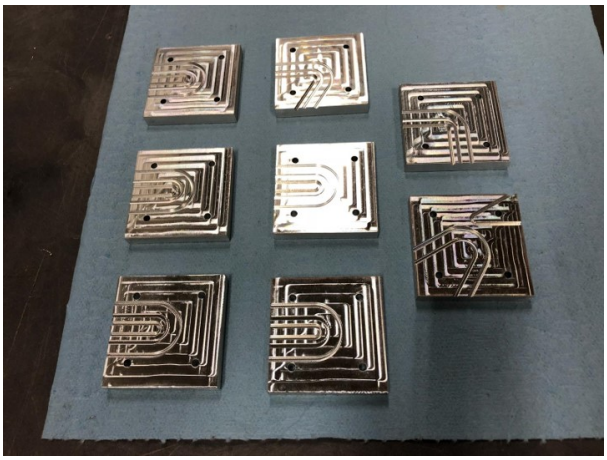

Figure 5: Annealing Mold Bases

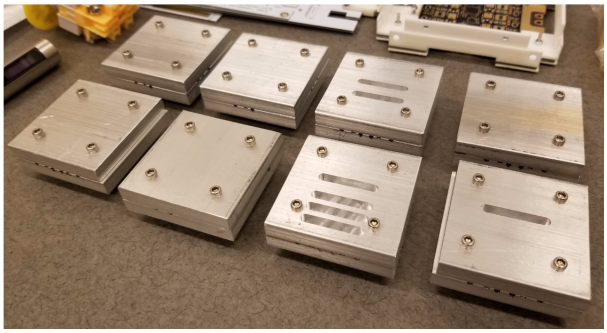

Figure 6: Annealing Mold Lids

we place the mold containing the SMA into the oven, leave it in there for 30 minutes, and quench it in cold water immediately after.

A range of annealing times was tested before finding that 30 minutes allowed the SMA to best maintain its remembered shape. Since overtraining the SMA strips was needed to actuate against the opposing SMA, Fig. 5 shows the different aluminum molds machined to find the appropriate overtraining angle. Similarly, Fig. 6 shows the process of determining the ideal number of slots in the mold lid to allow for quicker and better quenching. An overtrain angle of 0°, where the two ends of the SMA strip are held parallel, and a mold lid with 4 slots, provided the best remembered shape. The two halves of the mold were bolted together during annealing.[16]

Nitinol plates of 0.1 mm, 0.25 mm, and 0.5 mm thicknesses were tested in the hinge design. Since the SMA strips are in opposition to each other, each strip needed to exert enough force to actuate against the other SMA while remaining pliable. The 0.25mm thickness worked best with the hinge design.

Electrical Design

The electronics for driving the SMAs are designed to control power through four SMAs while providing power and hinge angle feedback. The current through each SMA is independently controlled via a PWM signal generated by an Arduino, which is used to set a desired average current. Joule heating due to this current creates a rise in temperature which causes the SMA to begin to actuate. Each hinge is actuated by two SMAs, with the low side of each SMA tied to a MOSFET with a gate driven by the Arduino PWM signal. The high sides of both SMAs on a hinge are tied together and in series with a shunt resistor, which allows for current measurement. Assuming only one SMA on a hinge is being driven at a time, the measured current will be the current through the driven SMA. When a power step input of 1 W is applied to one SMA on a fully assembled hinge, the angular velocity of the hinge reaches a maximum after approximately four seconds.

A single printed circuit board (PCB) was designed to integrate all components into a form that fits inside a 3U CubeSat. This board contains current and voltage feedback devices to calculate SMA power and resistance during operation. In addition, a SD card interface and accelerometer breakout board were included for additional data and recording capabilities during a microgravity flight test.

In order to accurately perform SMA power readings, the resistance of the system must be precisely characterized. The SMA resistance is on the same order of magnitude as the external resistance, where external resistance is defined as the resistance of all wires and connectors in series with the ends of the SMA strip. This includes the screws used to mount the SMA on the hinge, ring terminal connectors and wire connecting to the PCB. In order to accurately characterize this external resistance, a Kelvin four-wire resistance measurement is used. The resistance of the SMA is measured before integration, and the resistance of the SMA in series with the external resistance is measured after integration. The difference of the two measurements is recorded as the external resistance. This measurement is performed for each SMA following hinge electrical integration and used to calibrate the power and resistance calculation methods.

The accuracy of SMA power and resistance calculations performed by the Arduino in our current system is largely dependent on the accuracy of the Kelvin measurements. In addition, driving the SMAs at lower power levels increases error in the power calcu-

lation. An error analysis of the power calculation was performed by including the accuracy of all discrete components in the voltage and current sensing signal chain, including the shunt resistor, instrumentation amplifier, analog to digital converter (ADC), and low pass filter. The expected error in measured power and resistance values based on this analysis is included in the Results and Discussion section.

The power and resistance calculations are programmed into the Arduino. Fig. 7 shows the high level electronics schematic and the final printed circuit board assembly (PCBA). See Appendix A for detailed schematics and PCB gerber view files.

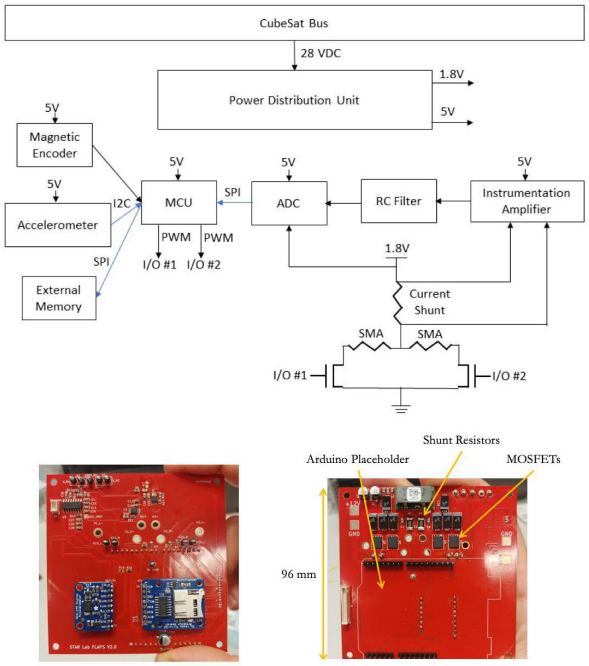

Figure 7: SMA driver electrical diagram and printed circuit board.

Controller Design and Implementation

The controller goals are to minimize the overshoot and maximize the actuation speed. The actuator should be able to reach a set point within 20 seconds and should not overshoot, in order to avoid unnecessary strain and heating from using both SMA strips in a single actuation. It is assumed that for small power inputs the transfer function is linear time invariant (LTI), allowing the use of linear control theory. Hysteretical features of SMA heating and cooling could also be safely ignored due to there being an antagonistic pair of SMAs, since cooling of

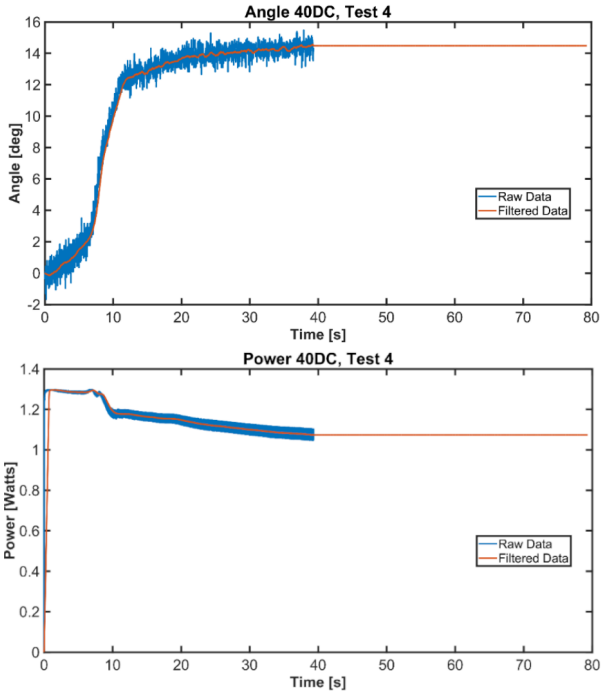

Figure 8: Angle and power during actuation test.

the SMA is never fundamental for actuation, only heating up the other SMA strip to push the hinge if necessary.

To determine the transfer function of the hinge, the step response of the actuation angle was measured at a constant duty cycle command from the Arduino. SMA resistance varies with its temperature, causing the power signal on the SMA strip to change as well. 25 tests were performed: 5 repetitions at 5 different duty cycles. Fig. 8 shows the measured power and angle as a function of time for one of the tests with 40% duty cycle.

The filter used in MATLAB to smooth the data is a moving-average with 200 samples. The transfer function is initially assumed to be a pure second order system with two poles. Initial tests showed a delay in actuation due to the SMA heating up to its transition temperature from room temperature. Lags were added to try to achieve a better fit but the increased complexity only slightly affected the function's fit accuracy, as shown in Fig. 9. This additional lag was neglected due to the marginal increase in fit accuracy, and so the second order transfer function as seen in Eq. 3[18] was used.

$$\frac{\theta(s)}{P(s)} = \frac{1.144}{s^2 + 0.183s + 0.01597} \tag{3}$$

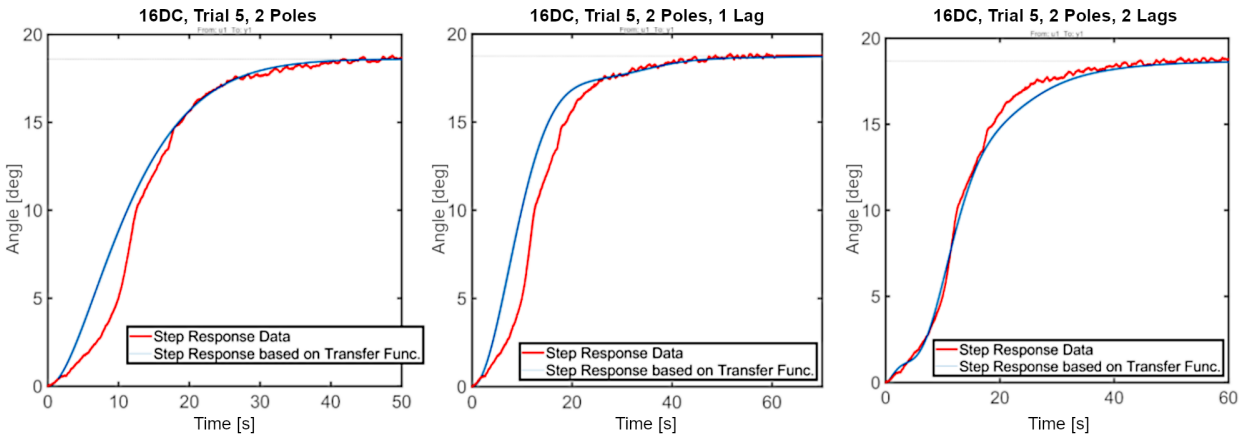

Figure 9: Comparison of transfer function fits, showing small improvements when additional poles and zeros are added.[18]

where θ is the actuation angle and s is the frequency domain in the s-plane, transformed from the time domain in the physical space.

Loop shaping was performed using the obtained transfer function in order to find gains for the proportional-integral-derivative (PID) controller that would give the fastest rise time without significant overshoot. Due to the neglected heating effects in the second order transfer function, it was anticipated that the antagonistic SMA pair would have a natural deadband, which would provide additional damping for small perturbations. Therefore, maximum overshoot was prioritized less than rise time since the overshoot would be damped in the actual system. Hence, maximum overshoot of 10% was deemed acceptable as an initial estimation.

After performing the loop shaping, the obtained gains were: $K_p = 0.04379$, $K_i = 0.002789$, and $K_d = 0.1442$.

The controller software was then converted into a discrete time system that could be implemented on the microcontroller. Integral and derivative terms were approximated in the z-plane by replacing the derivative with a second order finite difference approximation and replacing the integral term with a sum term instead, as shown in Eq. 4 and Eq. 5.

$$\frac{dx}{dt} \approx \frac{x[n] - 4x[n-1] + 3x[n-2]}{2\Delta t} \tag{4}$$

$$\int_0^t x(t)\,dx \approx \sum_{k=0}^{n} x[k]\Delta t \tag{5}$$

where $x(t)$ represents any arbitrary differentiable function of time, and $x[k]$ represents discrete samples of $x(t)$ at time $k\Delta t$.

An additional transfer function $\frac{DC(z)}{P(z)}$ was needed since the board controlled power indirectly by changing the duty cycle. It was also possible for an antagonistic SMA pair to have slightly different measured resistances due to the parasitic resistances of the wires and connectors being approximately on the order of the resistances of the SMAs themselves. This necessitated that the power to duty cycle conversion generalized well to a wide range of duty cycles and could track well regardless of a small difference in resistances of the two SMA strips.

Small transients due to parasitic effects of inductance and capacitance could be ignored in the 20-100ms timescales that the controller operated in, and so the discrete time poles of $\frac{DC(z)}{P(z)}$ could be approximated to be zero. Any root finding method could be used to quickly find the required duty cycle, but this option was dropped in favor of using a cascading PID-PI architecture, where the second PI loop functions as a power point tracker. This allowed reuse of controller code and easier stability analysis. Gains for this power point tracker were then found by modelling the system and linearizing it around a median power point that was determined to be approximately 0.5 W, since this was on the border of the linear and saturation regions. From this, K_{pp} was determined to be 15, and K_{ip} was determined to be 30.

Noisy measurements required additional filtering on the discrete-time controller. However, it was not possible or desirable to replicate the 200 point moving average filter used on the angle measurement when

analyzing the control system, due to the large amount of required memory and the incurred lag between the estimated angle and actual angle. Instead, a simple infinite impulse response low-pass filter was applied to update the angle estimate from the previous estimate and the new measurement as shown in Eq. 6. A value of 0.4 for the filtering parameter α was chosen after testing angle noise, due to its fast response time and much improved noise rejection over the unfiltered angle measurements. The same software-based filtering was also applied for power measurements, as well as the hardware RC filter on the PCB itself. After filtering, the derivative term was still found to be too noisy and causing random actuation of the antagonistic SMA since it was the dominant gain in the system. It was then removed, resulting in much smoother actuation, as shown in Fig. 13.

$$\hat{\theta}_n = \alpha \cdot \theta_n + (1 - \alpha) \cdot \hat{\theta}_{n-1} \tag{6}$$

where α represents how much of the new measurement θ_n is taken into account against a the current estimate $\hat{\theta}_{n-1}$ to generate the new estimate $\hat{\theta}_n$.

Additional clamping was incorporated into the discrete time controller, in order to prevent integral wind up and prevent the controller feedback path from summing up unrealistic values below or above the maximum and minimum suppliable power. A complete schematic of the discrete time controller can be seen in Fig. 10.

RESULTS AND DISCUSSION

Force Estimations

As discussed in the Mechanical Design section and Equations 1 and 2, the bending force of a SMA is derived from its Young's Modulus formulation, while the resisting force against its bending is calculated through the beam deflection formulation. The bending force for a 0.25 mm thick strip is calculated using Eq. 1 and the results can be seen in Fig. 11 for the bending force as a function of the power level and the actuation angle.[16]

To validate the calculations, a simple test was performed to measure the force applied by a bending SMA strip. A Futek load cell was hung from one end and the opposite end was connected to the hanging side of the SMA, as can be seen in Fig. 12. A mount for the SMA strips to hover below the load cell was designed and built, as can also be seen in Fig. 12. Both ends of the SMA were attached to a power supply that ran 1 W of power through the strips.

Two different thicknesses of SMA strips were tested: 0.25 mm and 0.5 mm. Both were tested in the position guided by the mounting, approximately 15°. The force measurement for the 0.25 mm thick strip was of 1.4 lbf, whereas the force for the 0.5 mm thick strip was of 3.2 lbf.

From the plot in Fig. 11, the expected bending force of the 0.25 mm thick strip at 15° is approximately 0.9 lbf, which is similar to the value measured in the experiments. The calculations and the experiments are not extremely precise, but having similar results is encouraging and supports the ballpark estimation.

From Eq. 2, the force necessary to bend the non-active SMA strip can be calculated based on the material and the geometry. The Young's Modulus being used is the one from the martensite state of the SMA, which is between 28 and 40 GPa. The width, the thicknesses, and the length of the strip are known, and the deflection can be calculated from the experimental set up. The resulting force required for bending is thus approximately 0.23 lbf for the 0.25 mm thick strip and 1.80 lbf for the 0.5 mm thick strip.

The comparison between the necessary bending force and the provided bending force for both thicknesses can be summarized as:

- 0.25 mm thick: provides 1.4 lbf and needs 0.23 lbf to be bent;
- 0.5 mm thick: provides 3.2 lbf and needs 1.80 lbf to be bent.

Fortunately, both thicknesses of SMA strips provided more bending force than necessary. As previously stated, the ratio between provided actuation force and necessary non-active force is more favorable for the smaller thicknesses, but the absolute force difference was larger in the thicker 0.5 mm strip. This opens some room for discussion, as different characteristics can be more valuable for different applications. In this study, focus was given to the 0.25 mm thick strip.

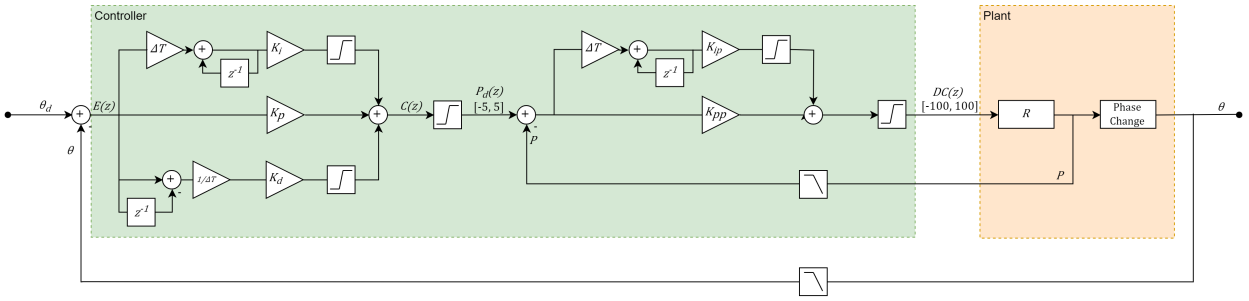

Figure 10: Diagram of discrete time controller implementation.

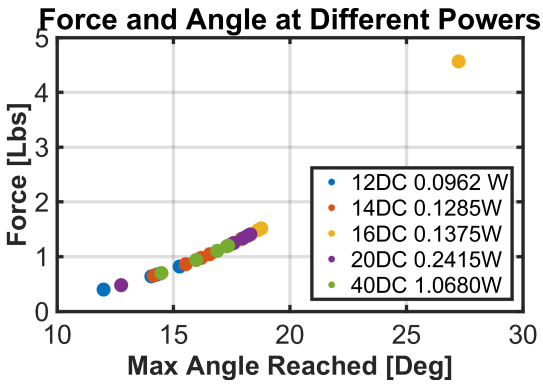

Figure 11: Estimation of the bending force at different power levels and actuation angles.

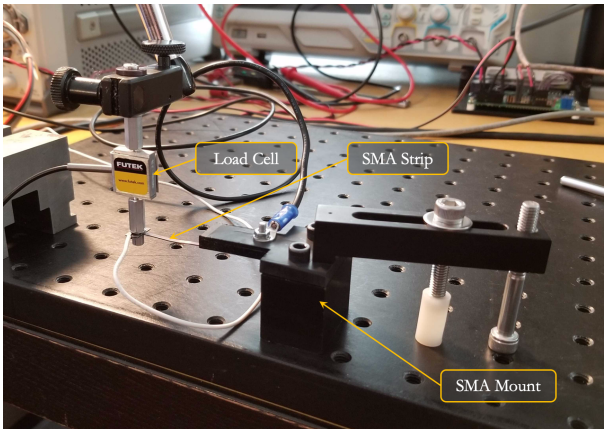

Figure 12: SMA bending force measurement using a load cell.

Actuator Performance with Current Design

The hinge mechanism provides 18° of reliable actuation in the current design. Friction and external damping forces were minimized to accommodate for the resistance of the SMAs when placed in an antagonistic arrangement. When actuating in opposition, buckling of the inactive SMA was the issue which further limited the actuation angle. Increasing the range of the hinge is the next step in developing this deployable actuator.

The SMA driver PCB measures power through a SMA with an accuracy of 5% at 1 W, and SMA resistance with an accuracy of 5% at 1 W. The measurement error decreases at higher power levels. While this accuracy analysis is based on component manufacturing specifications and electrical operating conditions, further hardware tests on the PCB should be performed to compare the Arduino program power calculations to the actual SMA power in order to fully characterize the SMA power measurement error. Measuring mean SMA power can be accomplished with a power analyzer or oscilloscope using a current probe and differential voltage probe. The voltage probe leads would need to make contact with the SMA strip at a point next to the screw holes on either end of the strip, which would likely require external wires to be soldered directly to the SMA in order to make a precise measurement of the potential difference. This power measurement scheme would account for parasitic inductance and capacitance in the SMA, which is likely a source of error in the Arduino based power calculation which simply multiplies SMA average current and average voltage to calculate power.

The controller tracked the predicted step response well after converging on an estimate for angle, and safely commanded up to the maximum 5 W of power to the SMA without it re-annealing. Overshoot and

damped oscillations were reduced compared to the predicted step response due to the natural dead band of the two SMA strips and to their initial lag to actuate, to the point where neither could be observed in the test, as can be seen in Fig. 13. A 10% to 90% rise time of 2.78 seconds was observed for the discrete time controller, and observed steady state error was minimal, with angle error noise being much more dominant.

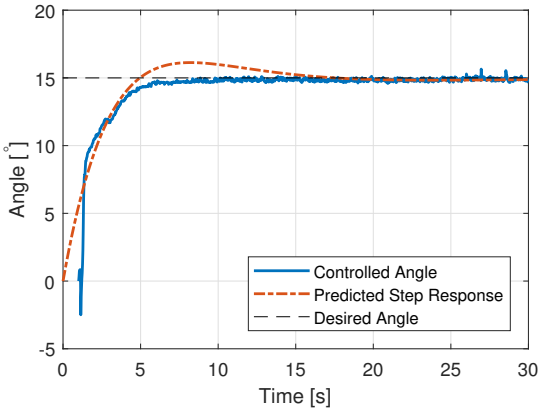

Figure 13: Response of the implemented discrete time controller compared to step response of model ($\Delta t = 20$ ms)

Future Work

The constraining and annealing methods are functional. The hinge mechanical design is limited, and future revisions will attempt to increase the angle range to the 90° demonstrated previously.[13] Round wires have the potential to exert a slightly higher torque before stagnation, but could present challenges with stowing the deployable without over-straining and damaging the SMA. A previous iteration of the hinge developed by Haughwout[19] used round wires constrained with 3D printed metal contacts and mounted on a PCB CubeSat endcap.[19] Actuation was demonstrated to 180°C without feedback control. Integration of the round wire design with the feedback control method could yield a more robust hinge with a larger range.

Temperature of solar panels in space can range between -100°C and up to 150°C,[20] highly dependent on satellite orientation. Shape memory alloys with higher transition temperatures could be implemented to provide further robustness against accidental actuation during orbit.[12] NASA Glenn Research Center has produced high temperature shape memory alloys with a transition temperature of 200°C,[21,22] which would allow controlled usage of SMA-based actuators in a space environment. Un-commanded actuation due to the surrounding temperature could potentially be used to automatically actuate deployables when facing the sun, making it a low power actuator. This would lower the power requirements of the actuator. Simulations of the SMA temperature in orbit should be performed before implementing the actuator in a satellite structure.

For controller improvements, state estimation with noisy measurements could be overcome with a simple one dimensional Kalman filter for angle and angular velocity measurements. This would allow use of the derivative term that was previously unusable due to the noise in the angle measurement that overpowered every other term in the controller, potentially allowing faster rise times on the discrete time controller.

A preheat loop that keeps the SMA just under its actuation temperature would also potentially allow faster rise times, however it is unknown how much this would improve rise time, as initially the controller commands the maximum power of 5 W, making the heat up time negligible. This would require characterizing the SMA's resistance-temperature curve, which could also be used to implement additional safety features for overheating protection.

The parabolic flight will help characterize the performance of the FLAPS mechanism in microgravity. The test will verify how the weight of the solar panel affects hinging capabilities and controller response.

CONCLUSION

A repeatable, precise, and controllable SMA hinge with limited actuation range between 0° (stowed position) up to approximately 18° (deployed position) was demonstrated in the rotary bending hinge design, with future work to improve actuation to more than 90°.

The bending mechanism exerted enough force to actuate against the opposing SMA with limited range: the active strip provides approximately 1.4 lbf of bending force, while the opposing strip offers approximately 0.23 lbf of resisting force, resulting in a positive net force capable of deploying the hinge.

Nitinol manufacturing methods were established without losing the shape memory effect of the SMA

through water jetting and oven annealing. The annealed SMA is able to reach angles close to the trained position when it is tested outside the hinge, showing the the annealing and shape memory affect are not issues.

Control of the angle of actuation was demonstrated with a 5% accuracy up to a 5 W power level and will be confirmed in a microgravity environment during parabolic flight testing.

The limited actuation angle at 18° motivates further design iterations with the goal of improving the actuation capabilities and range of operations, mainly due to the overconstraint encountered in the current hinge design.

REFERENCES

[1] P. Fortescue, G. Swinerd, and J. Stark. *Spacecraft Systems Engineering, Chapter 15, Pages 495-526*. 2011. John Wiley Sons, Ltd, Fourth edition.

[2] D. Hartl and D. C. Lagoudas. Aerospace applications of shape memory alloys. April 2007. In *Proc. Insitution of Mechanical Engineers, Part G: Journal of Aerospace Engineering*, USA.

[3] Shape memory alloys. NASA Technology Transfer Program, April 2019.

[4] I. Mihalcz. Fundamental characteristics and design method for nickel-titanium shape memory alloy. 2001. 1, 45(1), pp. 75-86.

[5] J. M. Jani, M. Leary, A. Subic, and M. A. Gibson. A review of shape memory alloy research, applications and opportunities. December 2013. *Materials and Design*, (56):1078-1113.

[6] TiNi Aerospace. Frangibolt. TiNi Aerospace, May 2019.

[7] A. Guzik and O. Benafan. Design and development of cubesat solar array deployment mechanisms using shape memory alloys. May 2018. In *Proc. 44th Aerospace Mechanisms Symposium*, pp. 375-388, NASA Glenn Research Center.

[8] Sierra Nevada Corporation. Space technologies product catalog. Space Systems, Louisville, CO, 2015.

[9] J. Cederstrom and J. Van Humbeeck. Relationship between shape memory material properties and applications. June 1995. Le Jounal de Physique IV, 05(C2), pp. C2-335-C2-341.

[10] H. Yuan, J. Faurous, F. Chapelle, and X. Balandraud. A review of rotary actuators based on shape memory alloys. 2017. Journal of Intelligent Material Systems and Structures, 28(14), pp. 1863-1885.

[11] Y. H. Teh. Fast, accurate force and position control of shape memory alloy actuators. June 2008. PhD thesis, The Australian National University, Canberra, ACT.

[12] W. Huang. Shape memory alloys and their application to actuators for deployable structures. page 192.

[13] M. O. Khatsenko. A rotary shape memory alloy actuator for cubesat deployable structures. June 2017. Master's thesis, Massachusetts Institute of Technology, Cambridge, MA.

[14] Super small non-contact rotary encoer rm08. https://www.rls.si/eng/rm08-super-small-contact-rotary-encoder, May 2019.

[15] Onyx 3d printer filament and printing material. markforged. Markforged Materials, May 2019.

[16] P. do Vale Pereira. Folded lightweight actuated position system (flaps) for cubesat deployables. June 2019. Master's thesis, Massachusetts Institute of Technology, Cambridge, MA.

[17] Nitinol innovation, development and supply. April 2019. Kellogg's Research Labs.

[18] M. M. Contreras. Design, analysis, and control of a nitinol shape memory alloy rotary actuator for spacecraft deployable structures. June 2019. Master's thesis, Massachusetts Institute of Technology, Cambridge, MA.

[19] C. Haughwout, D. Barnes, M. Khatsenko, J. Clark, and K. Cahoy. Folded lightweight aperture precision system. 2017.

[20] Tarun Ghosh. International space station thermally induced solar array base loads. 1997. Boeing North American, Inc.

[21] O. Benafan, G. S. Bigelow, M. Elahinia, N. S. Moghaddam, A. Amerinatanzi, S. Saedi, G. P. Toker, and H. Karaca. Additive manufacturing of nitihf high temperature shape memory alloy. 2017. NASA Technical Reports.

[22] Reinventing the wheel. NASA Glenn Research Center, April 2019.

APPENDIX A

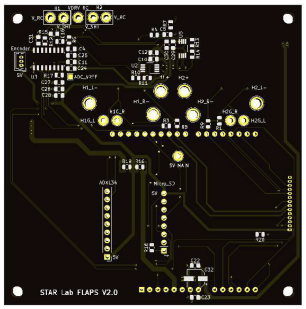

Figure 14: SMA Driver PCB (Bottom)

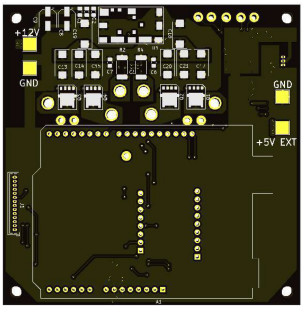

Figure 15: SMA Driver PCB (Top)

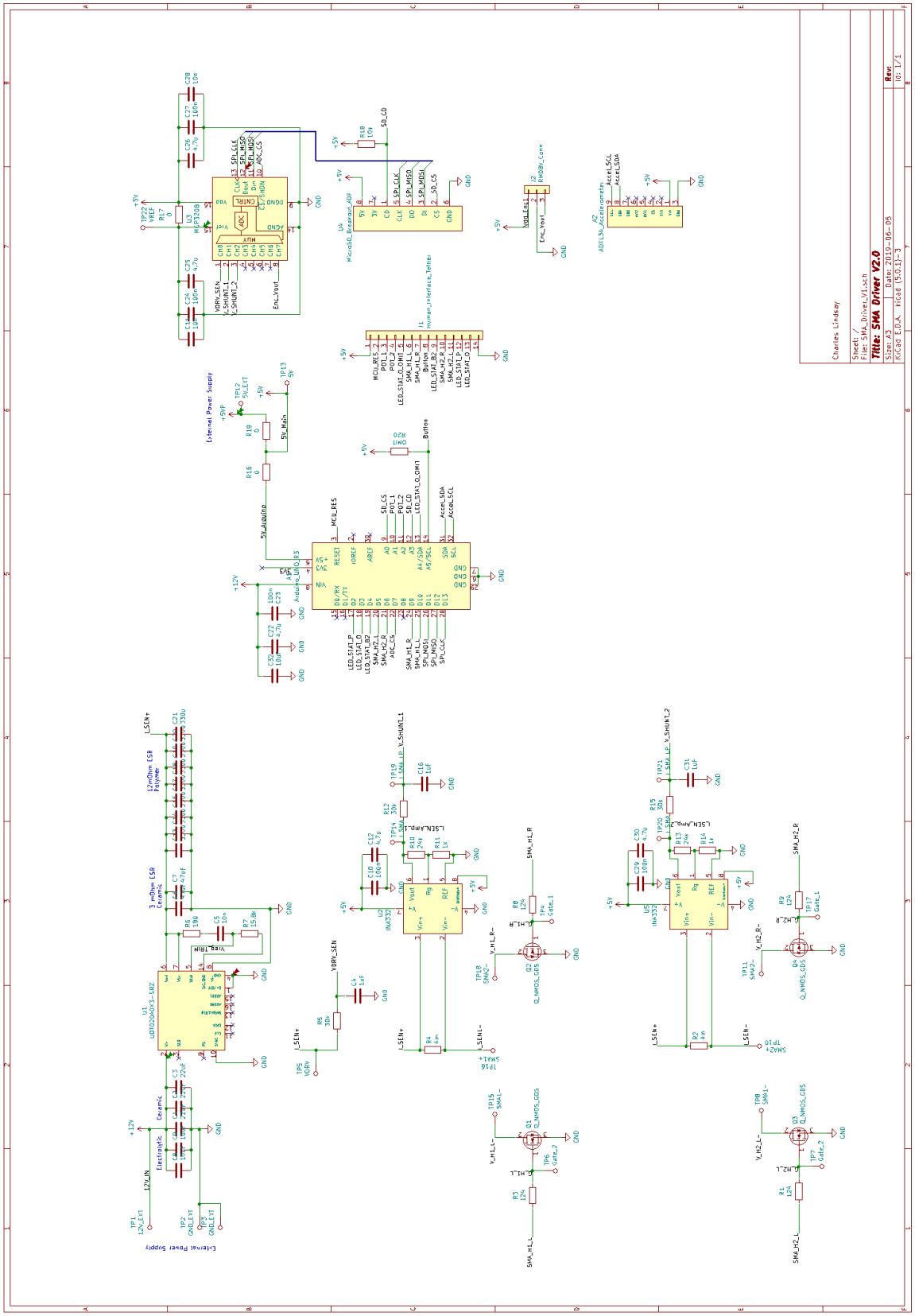

Figure 16: Full SMA Driver Schematic.